

Copper Binding Sites in the Manganese-Oxidizing Mnx Protein Complex Investigated by Electron Paramagnetic Resonance Spectroscopy

Lizhi Tao,[†] Troy A. Stich,[†] Shu-Hao Liou,^{†,‡} Alexandra V. Soldatova,^{‡,§} David A. Delgadillo,[§] Christine A. Romano,^{||} Thomas G. Spiro,[‡] David B. Goodin,[†] Bradley M. Tebo,^{||} William H. Casey,^{†,‡,¶} and R. David Britt^{*,†,‡}

[†]Department of Chemistry and [‡]Department of Geology, University of California, One Shields Avenue, Davis, California 95616, United States

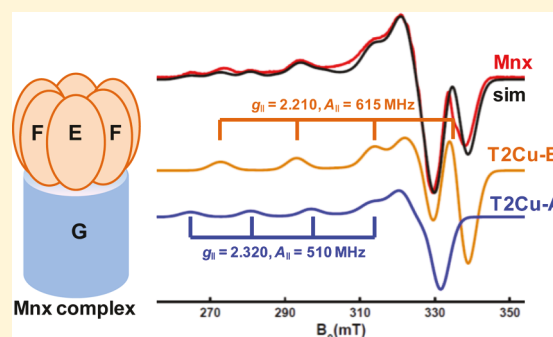
[§]Department of Chemistry & Chemical Biology, University of California, 5200 North Lake Road, Merced, California 95343, United States

^{||}Division of Environmental and Biomolecular Systems, Institute of Environmental Health, Oregon Health & Science University, Portland, Oregon 97239, United States

[‡]Department of Chemistry, University of Washington, Box 351700, Seattle, Washington 98195, United States

S Supporting Information

ABSTRACT: Manganese-oxide minerals (MnO_x) are widely distributed over the Earth's surface, and their geochemical cycling is globally important. A multicopper oxidase (MCO) MnxG protein from marine *Bacillus* bacteria plays an essential role in producing MnO_x minerals by oxidizing $\text{Mn}^{2+}(\text{aq})$ at rates that are 3 to 5 orders of magnitude faster than abiotic rates. The MnxG protein is isolated as part of a multiprotein complex denoted as "Mnx" that includes accessory protein subunits MnxE and MnxF, with an estimated stoichiometry of $\text{MnxE}_3\text{F}_3\text{G}$ and corresponding molecular weight of ≈ 211 kDa. Herein, we report successful expression and isolation of the MCO MnxG protein without the E_3F_3 hexamer. This isolated MnxG shows activity for $\text{Mn}^{2+}(\text{aq})$ oxidation to form manganese oxides. The complement of paramagnetic Cu(II) ions in the Mnx protein complex was examined by electron paramagnetic resonance (EPR) spectroscopy. Two distinct classes of type 2 Cu sites were detected. One class of Cu(II) site (denoted as T2Cu-A), located in the MnxG subunit, is identified by the magnetic parameters $g_{\parallel} = 2.320$ and $A_{\parallel} = 510$ MHz. The other class of Cu(II) sites (denoted as T2Cu-B) is characterized by $g_{\parallel} = 2.210$ and $A_{\parallel} = 615$ MHz and resides in the putative hexameric MnxE_3F_3 subunit. These different magnetic properties correlate with the differences in the reduction potentials of the respective Cu(II) centers. These studies provide new insights into the molecular mechanism of manganese biomineralization.



1. INTRODUCTION

Manganese-oxide minerals (MnO_x) widely distributed over the Earth's surface¹ participate in a wide variety of globally important geochemical processes. Manganese-oxide minerals photoreduce and dissolve in the upper photic zone of the ocean.² This dissolution is majorly counterbalanced by diurnal $\text{Mn}^{2+}(\text{aq})$ oxidation back to manganese-oxide solids,³ a process where microorganisms (bacteria and fungi)^{4,5} play an essential role. Aerobic biological $\text{Mn}^{2+}(\text{aq})$ oxidation in seawater (pH = 8.16) occurs at rates that are 3 to 5 orders of magnitude faster than abiotic pathways.⁶ In marine *Bacillus* species (PL-12, SG-1 and MB-7), one gene, *mnxG* encoding a putative multicopper oxidase (MCO),^{7–10} has been identified as being responsible for catalyzing the $\text{Mn}^{2+}(\text{aq})$ oxidation.^{9,10}

MCO enzymes contain three types of copper cofactors:^{11,12} type 1 (T1), or blue copper sites (coordinated in a trigonal pyramidal geometry by one cysteine and two histidine side chains), are characterized by an intense absorption feature at ≈ 590 nm which is assigned to a ligand-to-metal ($\text{Cys } S_{\pi} \rightarrow \text{Cu } 3d_{x^2-y^2}$) charge-transfer transition. Oxidized T1Cu sites are also known to give rise to Cu(II) electron paramagnetic resonance (EPR) signals with a small $^{63,65}\text{Cu}$ hyperfine coupling ($A_{\parallel} \approx 4\text{--}10$ mT). These spectroscopic properties are characteristic of the highly covalent Cu–Cys S bond. Type 2 (T2) copper sites (also known as “normal copper”) are often found in square-planar geometries. In MCOs, the T2Cu site is

Received: March 6, 2017

Published: June 6, 2017

coordinated by two histidines and an aquo-derived hydroxo ligand, with an open coordination site oriented toward the center of the trinuclear site, which is composed of a T2Cu site and a dinuclear T3Cu site (vide infra). When oxidized, these T2Cu sites are characterized by a $^{63,65}\text{Cu}$ hyperfine splitting ($A_{\parallel} \approx 20$ mT) which is much larger than in the T1Cu sites. The final type of copper cofactor in MCOs is a dinuclear copper center (type 3: T3), where in its resting state the two Cu ions are bridged by a hydroxide. The two Cu(II) ions in the oxidized T3 cluster are antiferromagnetically coupled and therefore EPR silent.^{11,12}

All three of these copper cofactors in MCOs (with a total of four Cu ions) are required for oxidase activity. During the catalytic cycle, T1Cu accepts electrons from the substrate and transfers them intramolecularly over ≈ 13 Å to the trinuclear T2/T3Cu site, where exogenous O_2 binds and is rapidly reduced to water (with a second-order reaction rate constant of $k_{\text{eff}} \approx 10^6 \text{ M}^{-1} \text{ s}^{-1}$).^{13–17} Some MCOs such as human ceruloplasmin have two extra T1Cu sites, giving a total of six copper ions per protein, although only one of the three T1Cu is redox-active during catalysis.^{14,18} The MCO enzyme CueO from *E. coli* has an extra Cu site that mediates electron transfer in order to oxidize bulky organic substrates that cannot access the T1Cu site directly.^{19–22} Phenoxazinone synthase has an extra T2Cu site, which functions to stabilize the quaternary structure of the hexamer.²³

The manganese oxidase MCO enzyme, MnxG protein, was recently isolated and purified as part of a multiprotein complex by coexpressing *mnxD* gene construct, denoted as Mnx, where it is combined with several copies of accessory protein subunits MnxE and MnxF.^{7,8,24} Recent mass spectrometric analysis show that the Mnx protein complex has a molecular weight of ca. 211 kDa,⁸ which may reflect a composition of one MnxG unit (≈ 138 kDa) along with, presumably, a hexamer of MnxE and MnxF (E_3F_3) subunits with a molecular weight of ca. 73 kDa.^{8,24} Notably, MnxG was not found to be stable in the absence of MnxEF.²⁵ Soluble MnxEF protein, however, has been purified as a putative E_3F_3 hexamer in the absence of MnxG protein, and it contains T2Cu sites of unknown function, which were investigated by EPR spectroscopy.^{8,24} This MnxEF protein cannot oxidize $\text{Mn}^{2+}(\text{aq})$,^{8,26} while the full Mnx complex rapidly produces MnO_x in the presence of O_2 .^{7,8,24,27} For the expression of Mnx protein complex, the gene *mnxD* was included in the gene construct, as *mnxD*, *mnxE*, *mnxF*, and *mnxG* are all conserved among the three *Bacillus* species (PL-12, SG-1, and MB-7).^{9,10} Previous studies show that MnxD protein with a molecular weight of ≈ 30 kDa was expressed at midsporulation to late sporulation stages.¹⁰ However, as no protein homologous to MnxD is known, the role of MnxD is still unknown.

Herein, we report successful expression of Mnx complex from a plasmid that did not contain the *mnxD* gene and note no difference in expression levels or resultant Mnx activity. Additionally, we have isolated a soluble form of MnxG protein, in the absence of MnxEF, which is active for $\text{Mn}^{2+}(\text{aq})$ oxidation. We characterize the MnxG Cu(II) centers using EPR spectroscopy and compare these signals to those in the full Mnx protein complex and those measured previously for MnxEF. This complementary EPR data set allows for spectroscopic assignment of the T2Cu sites on either the MnxG or MnxEF subunits.

2. EXPERIMENTAL PROCEDURES

2.1. Mnx Protein Complex Expression and Purification.

Mnx protein complex ($\text{MnxE}_3\text{F}_3\text{G}$, ≈ 211 kDa) was expressed using a

mnxEFG gene construct, which is inserted in a Strep-tag II containing (pASK/IBA3plus) vector. This *mnxEFG* gene construct containing plasmid was built by removing the *mnxD* gene from the starting plasmid with the *mnxDEF* gene construct reported earlier.⁸ Specifically, the *mnxDEF* gene construct (NCBI accession EF158106) was first amplified from genomic DNA of *Bacillus* sp. PL-12 (taxonomy ID: 161537) by using the following primers: forward 5'-**CCGCGGTATGCGTCATTCGGATTATTTGAAAAA-TTTGT**-3' and reverse 5'-**GTCGACTGCCTTTTCTTCATTGTC-CCACC**-3', where in bold denotes the SacII and SalI restriction endonuclease sites used for cloning. The resulted amplicons were ligated into pJet1.2 (Thermo) entry vector and then cloned by restriction enzyme digestion and ligation into the pASK/IBA3plus vector with the Strep-tag II (underlined) fused to the C-terminus of MnxG through a linker (italic, *VDLQGDHLSAWSHPOFEK*). With this starting plasmid (pASK/IBA3plus with *mnxDEF* insert) in hand, to exclude the *mnxD* gene, only the *mnxEFG* insert and the vector were amplified by AccuPrime Pfx SuperMix (Thermo Fisher) using the following primers: forward 5'-GACATAAATTGCAGAAATTTT-ATTTACAAGAAAG-3' and reverse 5'-ACCGCGGTCTCCCAT-TTG-3'. The PCR product was purified by electrophoresis, phosphorylated by using T4 Polynucleotide Kinase (New England Biolabs, NEB, MA), ligated by using T4 DNA ligase (NEB), and then transformed into *E. coli* DH5 α competent cells (see [Supplementary Methods](#) for details). The final DNA was purified by Miniprep Kit (QIAGEN) and sequenced by UC Davis DNA sequencing facility with the forward primer (5'-GAGTTATTTTACCCTCCCTATCAG-3') and the reverse primer (5'-ACGCAGTAGCGGTAACGGC-3').

The Mnx protein complex was expressed and purified by optimizing previous methods described in ref 8 using the plasmid of *mnxEFG* gene construct inserted pASK/IBA3plus vector described above. This plasmid was transformed into *E. coli* BL21(DE3) and grown by shaking (≈ 200 rpm) at 37 °C to an O.D.₆₀₀ ≈ 0.5 – 0.6 in a Luria-Bertani (LB) broth containing 0.2 mM CuSO_4 and 100 mg/L ampicillin. The cells were then cooled down to 17 °C on ice (≈ 20 min) and induced by adding 100 μL 2 mg/mL anhydrotetracycline. Protein expression was continued for 18 h by shaking (≈ 180 rpm) at 17 °C. Then, CuSO_4 was added into the culture to a final concentration of 2 mM and the shaking function was turned off for another 22–24 h at 17 °C, in order to enable the microaerobic uptake of copper ions into the *E. coli* cytoplasm as described by Durão et al.²⁸

The cells were harvested by centrifugation ($6000 \times g$ at 4 °C for 30 min) and resuspended in Strep-tactin equilibration buffer (20 mM Tris-HCl, 150 mM NaCl, pH = 8.0, and 50 μM CuSO_4) supplemented with 10 mM CaCl_2 , 1 mM CuSO_4 , and an EDTA-Free SIGMAFAST Protease Inhibitor Cocktail Tablet. The cells were lysed by two rounds of French press at 1000 psi, and the crude extract was clarified by heat denaturation at 70 °C for 15 min. The cell debris was removed by centrifugation ($13000 \times g$ at 4 °C for 30 min), and the supernatant was filtered through a 0.4 μm pore polyvinylidene fluoride (PVDF) filter. The clarified supernatant was added to a 10 mL column volume (CV) of Strep-tactin Superflow Plus resin (QIAGEN) and slowly rotated for 1 h at room temperature. The unbound protein fraction was removed by gravity flow through the resin, and the resin was washed with 100 mL Strep-tactin equilibration buffer. The Mnx protein fraction was eluted by adding 50 mL 2.5 mM *d*-desthiobiotin in Strep-tactin equilibration buffer. The resin was regenerated with 200 mL 1 mM 2-(4-hydroxyphenylazo)benzoic acid and washed with 500 mL Strep-tactin equilibration buffer. The eluted Mnx protein fraction was concentrated to <1.0 mL in the filtration with 100 kDa molecular weight cutoff (Millipore) and loaded into HiLoad 16/600 Superdex 200 pg (GE Healthcare) equilibrated with 20 mM HEPES buffer (pH 7.8) with 50 mM NaCl and 5% D-glucose (weight/volume) at 4 °C.

Fractions corresponding to a single broad peak (≈ 211 kDa protein complex) were collected, concentrated, and dialyzed three times, at least 3 h each, with a volume of 1 L 20 mM HEPES pH 7.8, 50 mM NaCl for every 1 mL of protein sample at 4 °C. The protein was further dialyzed with 500 mL 20 mM Tris-HCl pH 8.0, 50 mM NaCl for 1–2 h in order to remove exogenous Cu(II) to give a clean EPR

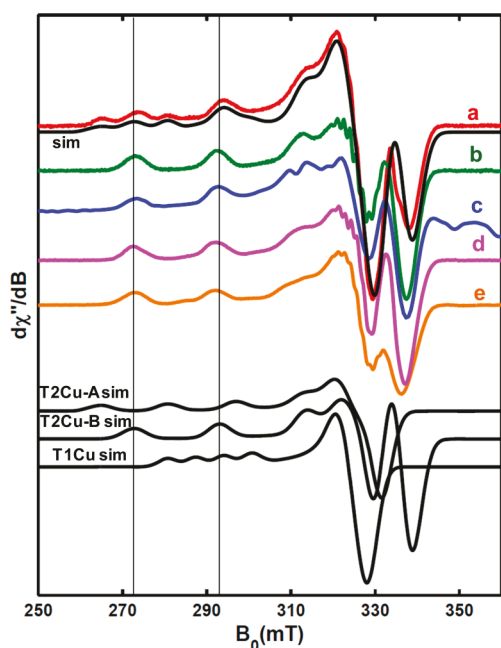


Figure 1. X-band CW EPR spectra of (a) as-isolated Mnx protein complex (red trace), (b) the Mnx protein complex that was anaerobically reduced with 24 equiv of $(\text{NH}_4)_2\text{Fe}(\text{SO}_4)_2$ (green trace), (c) fully reduced Mnx protein complex that was anaerobically oxidized by Mn(III)PP (blue trace), (d) the Mnx protein complex has been dialyzed with 50 mM Tris-buffer for 6 h (magenta trace), and (e) the as-isolated wild-type MnxEF protein. Experimental parameters: temperature = 15 K; microwave frequency = 9.38 GHz; microwave power = 0.02 mW (no saturation); conversion time = 40 ms; modulation amplitude = 0.8 mT; and modulation frequency = 100 kHz. Bottom three black traces are simulations of three Cu(II) species obtained using the following magnetic parameters: $g = [2.055 \ 2.320]$ and $^{65}\text{Cu} A = [54 \ 54 \ 510]$ MHz corresponding to T2Cu-A; $g = [2.046 \ 2.046 \ 2.210]$, $^{63}\text{Cu} A = [54 \ 54 \ 615]$ MHz corresponding to T2Cu-B; and $g = [2.050 \ 2.065 \ 2.305]$, $^{63}\text{Cu} A = [45 \ 45 \ 210]$ MHz corresponding to T1Cu site. Simulation of the spectrum of as-isolated Mnx (top black trace), denoted as “sim”, sums these three contributions with the ratio 2:3:1 of T2Cu-A:T2Cu-B:T1Cu.

spectrum (≈ 6 Cu(II)/Mnx, red trace in Figure 1). The protein was quantified by the Thermo Scientific Pierce bicinchoninic acid (BCA) protein assay or by the measured extinction coefficient of T1Cu ($5600 \text{ M}^{-1} \text{ cm}^{-1}$ for A_{590}) in the Mnx protein complex, giving a yield of ≈ 2 mg/L culture. The final protein was flash frozen in liquid nitrogen and stored at -80 °C.

2.2. MnxG Protein Expression and Purification. A plasmid with *mnxG* gene construct inserted into Strep-tag II (pASK/IBA3plus) containing a vector was built from the above plasmid with a *mnxEFG* gene construct. Only the *mnxG* gene and the vector were amplified by AccuPrime Pfx SuperMix (Thermo Fisher) using the following primers: forward 5'-ATGTTACGAAAATTCATGTTGTCGG-3' and reverse 5'-ACCGCGGTCTCCCATTTG-3'. The PCR product was purified by electrophoresis, phosphorylated by using T4 Polynucleotide Kinase (NEB), ligated by using T4 DNA Ligase (NEB), and then transformed into *E. coli* DH5 α competent cells. The final DNA was purified by Miniprep Kit (QIAGEN) and sequenced by UC Davis DNA sequencing facility with the forward primer (5'-GAGTTATTTTACCACCTCCCTATCAG-3') and the reverse primer (5'-ACGCAGTAGCGGTAACGGC-3').

The procedure for expressing and purifying MnxG protein is similar to that for the Mnx protein complex (see Supplementary Methods for the whole procedure), except that no heat denaturation (at 70 °C) was used. (Note: this is essential for isolating the soluble MnxG protein.) The molecular weight of the MnxG protein (≈ 138 kDa) was confirmed

by running Bis-Tris (4–12%) sodium dodecyl sulfate polyacrylamide electrophoresis gel (SDS–PAGE, Bio-Rad) followed by staining the gel with Coomassie Blue. The protein was quantified by Thermo Scientific Pierce BCA protein assay, giving a yield ≈ 0.2 mg/12 L culture. Final protein was flash frozen in liquid nitrogen and stored at -80 °C.

2.3. MnxEF Protein Expression and Purification. The MnxEF protein (shown to be a hexamer with E_3F_3 stoichiometry) was expressed and purified by previous methods described in ref 8 using the plasmid of gene construct *mnxEF* inserted into pASK/IBA3plus vector. The purification procedure is similar to that for purifying Mnx protein complex (see Supplementary Methods for details), except the different Strep-tactin equilibration buffer (100 mM Tris-HCl pH 8.0 and 150 mM NaCl) was used. The heat denaturation at 70 °C for MnxEF protein was also omitted. The protein was dialyzed with buffer solution of 50 mM Tris-HCl pH 8.0 and 50 mM NaCl for three times (3 h each). The protein was quantified by Thermo Scientific Pierce BCA protein assay. The final protein was flash frozen in liquid nitrogen and stored at -80 °C.

2.4. Reconstitution of Mnx Protein Complex. The Mnx protein complex (500 μL 10 μM) was dialyzed with 500 mL 50 mM Tris-HCl pH 8.0, 50 mM NaCl at 4 °C for 6 h. The sample was concentrated, followed by fresh buffer (20 mM HEPES, 20 mM NaCl, pH = 7.8, 20% ethylene glycol) exchange four times using 0.5 mL centrifugal filters (Amicon Ultra, #UFC510024). The final concentrated sample (200 μL 25 μM) was transferred to the bottom of the quartz X-band EPR tube (Wilmad PQ-706, i.d. = 2.8 mm, o.d. = 3.8 mm) using a glass pipet, frozen in liquid nitrogen and checked by CW EPR spectroscopy. The sample was then thawed and reconstituted by adding six equivalents of CuSO_4 to the protein sample for 30 min equilibration, followed by fresh buffer (20 mM HEPES, 20 mM NaCl, pH = 7.8, 20% ethylene glycol) exchange four times to remove exogenous Cu(II). The final concentrated sample (200 μL of 25 μM) was transferred to EPR tube, frozen in liquid nitrogen, and measured by CW EPR spectroscopy.

2.5. Reduction of Mnx Protein Complex by Fe(II). Reduction of Mnx by Fe(II) was performed anaerobically in a glovebox that had been purged with N_2 . First, at room temperature (22 °C), 150 μL Mnx (100 μM) in a deoxygenated HEPES-buffered solution (20 mM HEPES, 20 mM NaCl, pH = 7.8, 20% ethylene glycol) was transferred to the EPR tube. Then 10 μL $(\text{NH}_4)\text{Fe}(\text{SO}_4)_2 \cdot 6\text{H}_2\text{O}$ (9.0 mM) in a deoxygenated buffer solution (20 mM HEPES, 20 mM NaCl, pH = 7.8) was transferred by glass pipet to mix with Mnx protein for 15 min in the X-band EPR tube before being frozen in liquid nitrogen. This sample was denoted as “6 Fe(II) + Mnx” and measured by CW EPR spectroscopy. This sample was then thawed in the glovebox. Another 10 μL $(\text{NH}_4)\text{Fe}(\text{SO}_4)_2 \cdot 6\text{H}_2\text{O}$ (9.0 mM) in buffer solution (20 mM HEPES, 20 mM NaCl, pH = 7.8) was transferred by glass pipet to mix with the “6 Fe(II) + Mnx” for 15 min in the X-band EPR tube before being frozen in liquid nitrogen. This sample was denoted as “12 Fe(II) + Mnx” and checked by CW EPR spectroscopy. The reduction procedure was repeated for another two times, yielding spectra of samples denoted “18 Fe(II) + Mnx” and “24 Fe(II) + Mnx”.

2.6. Oxidation of the Fully Reduced Mnx Protein Complex by Mn(III)PP. First, fully reduced Mnx protein was prepared anaerobically in a glovebox that had been purged with N_2 . 10-Fold excess of sodium dithionite was added to Mnx protein solution and allowed to react for 30 min during which the blue color from the T1Cu center ($\lambda_{\text{max}} = 590$ nm) was bleached. Excess sodium dithionite was removed by desalting the solution using a spin column (Thermo Scientific, no. 89849) that had been pre-equilibrated with deoxygenated HEPES-buffered solution. 3-Fold exchange of the buffer was accomplished using 0.5 mL centrifugal filters (Amicon Ultra, no. UFC510024). The resulting reduced protein was checked by X-band CW EPR spectroscopy for residual signals from Cu(II)-containing species. No such signals were observed, indicating that all the Cu(II) centers in Mnx were fully reduced by the treatment. This fully reduced protein complex is denoted as “RedMnx”.

Mn(III)PP (pyrophosphate) was prepared aerobically by adding Mn(III) acetate to the $\text{Na}_4\text{P}_2\text{O}_7$ buffer solution (20 mM HEPES,

20 mM NaCl, pH = 7.8). The precipitation was filtered away using a 0.4 μm pore PVDF filter. The concentration of the obtained transparent pink solution of Mn(III)PP was calculated via the extinction coefficient $\epsilon_{258\text{ nm}} = 6750\text{ M}^{-1}\text{ cm}^{-1}$.²⁹ Before being transferred to the glovebox, Mn(III)PP solution was sparged with argon for 0.5 h.

A reaction sample was prepared by transferring 100 μL of 100 μM fully reduced Mnx protein to an EPR tube, followed by addition of 100 μL of 200 μM deoxygenated Mn(III)PP buffer solution. After ≈ 15 min, this sample was frozen in liquid nitrogen and checked by CW EPR spectroscopy.

2.7. UV–visible Absorption Spectroscopy. Absorption spectra of the protein samples (i.e., Mnx complex and MnxG protein) were recorded on an Agilent 8453 UV–visible absorption spectrophotometer in a 1 cm path length quartz cuvette (180 μL volume). The buffer of 20 mM HEPES, 20 mM NaCl, pH = 7.8, 20% ethylene glycol was used. All the UV–vis spectra in this work were collected at room temperature (24–26 $^{\circ}\text{C}$).

2.8. Reaction Assay of MnxG Protein and Kinetics Analysis. $\text{Mn}^{2+}(\text{aq})$ oxidation by MnxG protein was monitored via absorption spectroscopy obtained with an Agilent 8453 UV–vis spectrophotometer, using a thermostatable multicell configuration with automated kinetic scan capability and 1 cm path length cuvettes (1 mL volume). The samples were continuously stirred with a Spinette magnetic stirrer (Starna Cells, Atascadero, CA) at room temperature.

Reaction assays (1 mL volume) contained 48 nM MnxG in 10 mM HEPES buffer, pH 7.8. Mn(II)-oxidation reaction was initiated by adding an appropriate volume of 0.01 M MnSO_4 stock solution directly to the cuvette with enzyme, and the evolving spectra due to MnO_2 product were acquired every 10 s under both UV and vis lamps. The 10 s acquisition time was thought to minimize the photo-oxidative effect of HEPES.^{30–33}

To process the data, the protein spectrum (a small UV contribution at 280 nm) was subtracted from the evolving spectra, and an absorbance increase at a chosen wavelength was converted to MnO_2 concentration, assuming a full conversion of $\text{Mn}^{2+}(\text{aq})$ substrate to the MnO_2 product at the end of the reaction when the absorbance reached a plateau. In this work, the early reaction manganese oxide product was monitored by the absorbance at 240 nm, where the effect of MnO_2 nanoparticle growth (broad band ~ 350 nm) was minimized (see refs 30 & 34 for more details). The $[\text{MnO}_2]$ versus time (x, second) curve was fitted to the eq 1 for activated enzymes:

$$[\text{MnO}_2] = V_{s-s} * (x - x_0) - \frac{V_{s-s}}{k_{\text{act}}} * [1 - e^{-k_{\text{act}} * (x - x_0)}] \quad (1)$$

where k_{act} is the rate constant for enzyme activation, and V_{s-s} is the subsequent steady-state velocity. x_0 is the lag before reaction starts and is optimized in the fitting procedure.

2.9. EPR Spectroscopy. The X-band (9.38 GHz) continuous-wave (CW) EPR spectra were recorded on a Bruker (Billerica, MA) EleXsys E500 spectrometer equipped with a superhigh Q resonator (ER4122SHQE). Cryogenic temperatures were achieved and controlled using an ESR900 liquid helium cryostat in conjunction with a temperature controller (Oxford Instruments ITC503) and gas flow controller. CW EPR data were collected under slow-passage, non-saturating conditions. The spectrometer settings were as follows: conversion time = 40 ms, modulation amplitude = 0.8 mT, and modulation frequency = 100 kHz; other settings are given in corresponding figure captions. Spin quantification was determined by comparison of the double integral intensity of the EPR spectra to that of a standard solution of 100 μM CuSO_4 with 200 μM HCl, 200 mM NaClO_4 , and 20% ethylene glycol (see Figure S1 and captions for details).³⁵

Q-band two pulse electron spin–echo (ESE)-detected field swept EPR spectrum ($\pi/2$ - τ - π - τ -echo) was collected at 34.322 GHz using a Bruker (Billerica, MA) EleXsys E-580 spectrometer equipped with a 1 W amplifier and an R.A. Isaacson cylindrical TE011 resonator in an Oxford CF935 cryostat. Pulse sequences were programmed with the PulseSPEL programmer via the XEPR interface. Experiment parameters: 30 K, microwave frequency = 34.322 GHz, $\pi/2 = 12$ ns,

and $\tau = 300$ ns. Spectral simulations were performed using the Easyspin 5.0 toolbox^{36,37} within the MatLab software suite (The Mathworks Inc., Natick, MA).

3. RESULTS

The Mnx complex ($\text{MnxE}_3\text{F}_3\text{G}$, ≈ 211 kDa) contains a variety of copper centers, but the role that each of these sites plays in manganese oxidation is unclear. Our goal here is to identify the EPR spectroscopic signature for each type of copper site and locate it within the Mnx complex. To do so, we first explored the effect of the MnxD gene product has on expression of the Mnx complex (section 3.1). It was also valuable to ascertain whether all the distinct EPR signals in the full Mnx complex can be identified in separately isolated subunits. The expression and isolation of MnxEF protein has been reported previously,⁸ but thus far MnxG has eluded isolation. In section 3.2, we describe a procedure for generating a small amount of soluble MnxG and discuss its activity for manganese oxidation in addition to its spectroscopic properties. Finally in section 3.3, we use the EPR spectra of MnxEF, MnxG, and chemically treated Mnx to assign each of the components to EPR spectrum of full Mnx complex.

3.1. Role of *mnxD* Gene. The gene of *mnxD*, *mnxE*, *mnxF*, and *mnxG* are all conserved among the three *Bacillus* species (PL-12, SG-1, and MB-7).⁹ Previous studies show that the active Mnx protein complex ($\text{MnxE}_3\text{F}_3\text{G}$, ≈ 211 kDa) could be expressed and purified by using a plasmid containing a gene construct of *mnxDEFG* from *Bacillus* sp. PL-12.^{7,8,27} However, the role of *mnxD* gene in the expression and purification or function of Mnx complex is currently unknown. Protein SDS–PAGE gel and amino acid sequence analysis⁹ results show that the expressed MnxD protein has a molecular weight of ≈ 30 kDa. MnxD was found mostly in the eluted unbound protein fraction (Figure S2, lane e), which was collected from the supernatant after gravity-flow through the Strep-tactin resin. This result suggests that the MnxD protein unit does not bind with the final Mnx complex (consistent with the results reported in refs 24 and 25), which is confirmed by the final Mnx complex SDS–PAGE bands with MnxE (≈ 12 kDa), MnxF (≈ 12 kDa), and MnxG (≈ 138 kDa) presented (Figures S2 and S3). Further, to test if the MnxD protein helps the over-expression of the Mnx complex, a plasmid with a gene construct of *mnxEFG* (no *mnxD*) was made (Figure S3). The final yield of the Mnx protein complex was comparable to the yield by using the plasmid with gene construct of *mnxDEFG* (approximately ≈ 2 mg protein per liter culture). Thus, we inferred that MnxD protein does not affect the expression, yield, and activity (vide infra) of the Mnx protein complex. Therefore, in this work, we employed the plasmid with gene construct of *mnxEFG* to express and isolate the stable active Mnx protein complex.

3.2. Isolation of MnxG Protein. Gene-alignment analysis shows that *mnxG* encodes a MCO, as there are motifs for T1Cu, T2Cu, and T3Cu binding.⁹ Previously, MnxG protein alone has not been successfully isolated. Now, however, we have expressed the MnxG protein, in the absence of MnxEF, using a plasmid with only the gene construct of *mnxG*. The corresponding SDS–PAGE gel (Figure S4 and S5) indicates that MnxG protein is expressed in *E. coli* BL23(DE3), as observable in the whole cell (Figure S4, lane b) and lysate (Figure S4, lane c). However, when the cell debris is removed by centrifugation ($13000 \times g$ at 4 $^{\circ}\text{C}$ for 30 min), most of the MnxG protein was found within inclusion bodies (Figure S4, lane e); however, a small amount of soluble MnxG protein

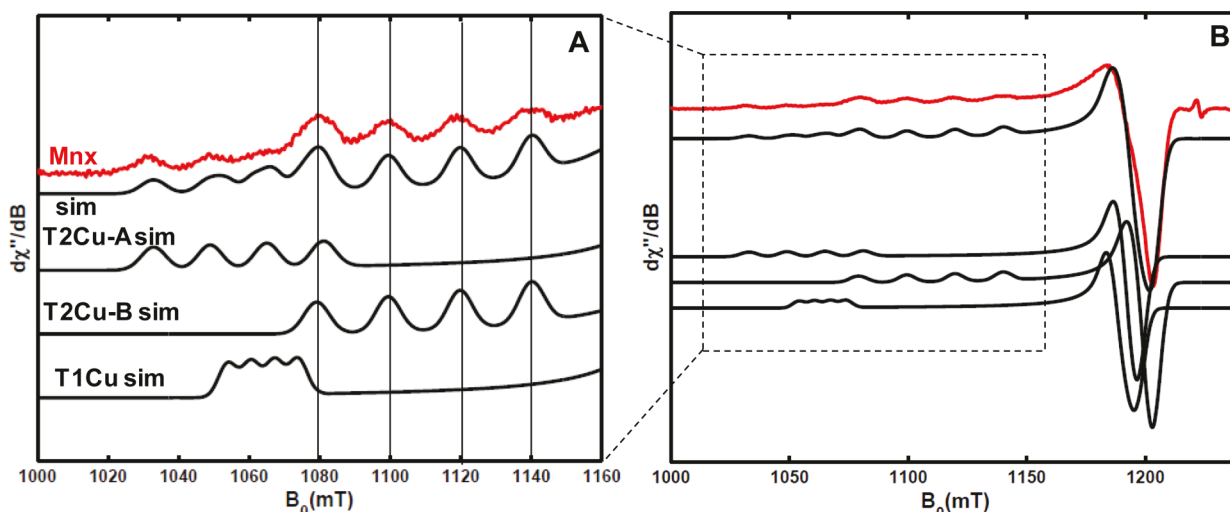


Figure 2. Q-band (34.322 GHz) pseudo-modulated (modulation amplitude, 1.0 mT) electron spin-echo (ESE) detected field swept EPR spectrum (red trace) of MnX protein complex (240 μ M) at 30 K, microwave frequency = 34.322 GHz, $\pi/2 = 12$ ns, and $\tau = 300$ ns. (A) is the zoom in g_{\parallel} range (the black dash rectangle) of the full spectrum in (B). The corresponding ESE detected field swept EPR spectrum is shown in Figure S6. The bottom three black traces are simulations of three Cu(II) species (T2Cu-A, T2Cu-B, and T1Cu) using the same magnetic parameters described in the caption of Figure 1. Simulation of the spectrum of as-isolated MnX (top black trace), denoted as “sim”, sums these three contributions with the ratio 2:3:1 of T2Cu-A:T2Cu-B:T1Cu. The small signal at $g = 2.0$ (1226.1 mT) is the quartz radical.

exists in the supernatant (Figure S4, lane d). The small fraction of soluble MnXG protein in the supernatant was purified by using Strep-tactin affinity resin (see Supplementary Methods for details), with a low yield of ≈ 0.2 mg per 12-liter culture. Unlike the whole MnX protein complex, MnXG denatures at high temperature (70 $^{\circ}$ C for 15 min), and as shown in Figures S4 (lane f), there is no soluble MnXG protein present in the heated supernatant; this is in contrast to the whole MnX protein complex. This temperature instability could be why MnXG had not been isolated previously.

3.3. EPR Characterization of Copper Sites in the MnX Protein Complex. In our initial EPR characterizations of the MnX complex, there were nonspecifically bound or exogenous Cu(II) centers contributing to the spectrum of the MnX protein (≈ 10 mononuclear Cu(II) centers per MnX complex).²⁷ We now have a procedure for removing these adventitiously bound copper centers via dialysis with a buffered solution of 20 mM Tris-HCl pH 8.0, 50 mM NaCl for 1–2 h (see Experimental Procedures for details), without affecting the $\text{Mn}^{2+}(\text{aq})$ oxidation activity of MnX protein complex. The resulting Tris-dialyzed, as-isolated MnX protein complex has been analyzed by both X-band (9.38 GHz) and Q-band (34.32 GHz) EPR spectroscopy, with the corresponding spectra shown in Figure 1 (red trace) and Figures 2, S6 and S7 (red trace), respectively. Spin quantification via EPR reveals ≈ 6 mononuclear Cu(II) centers per intact MnX protein complex. As the oxidized dinuclear T3Cu sites in the MCO MnXG unit are antiferromagnetically coupled and EPR-silent, only the oxidized T1Cu and T2Cu in the MCO MnXG unit as well as the oxidized T2Cu sites in the MnxEF subunit contribute to the EPR spectrum of the MnX complex. In what follows, we untangle the CW EPR spectrum of MnX, identifying which signals correspond to individual copper centers in the protein complex.

The EPR signal for the T1Cu was assigned previously by comparing the EPR spectrum of wild-type MnX with that of the MnXG H340A mutant complex (Note: His340 was identified as a putative ligand to the only T1Cu site in MCO MnXG subunit by gene sequence alignment).²⁷ The difference spectrum of

wild-type MnX and H340A complex corresponds to a Cu(II) center with $g_{\parallel} = 2.305$, $^{63}\text{Cu } A_{\parallel} = 210$ MHz values that are typical of type 1 blue-copper sites.

We distinguish two classes of T2Cu signals in the spectrum of the MnX complex (Figures 1 and 2). One class of T2Cu signals, denoted as T2Cu-A, is characterized by the axial g -values with $g_{\parallel} = 2.320 > g_{\perp} = 2.055$, consistent with a $d_{x^2-y^2}$ ground state description, as expected for a normal square-planar coordinated Cu(II) species.³⁸ A quartet of $^{63,65}\text{Cu}$ hyperfine lines is centered at 315.0 mT, corresponding to the g_{\parallel} value, with splittings of approximately 510 MHz (≈ 15.8 mT). The other class of T2Cu signals, denoted as T2Cu-B, has axial g values of $g_{\parallel} = 2.210 > g_{\perp} = 2.046$, which also points to a $d_{x^2-y^2}$ ground state³⁸ and an A_{\parallel} value of 615 MHz (≈ 19.8 mT) (Figures 1 and 2).

To determine where the two classes of T2Cu sites are located within the MnX complex, we compare the EPR spectra of the isolated subunits (i.e., MnxEF and MnXG) to that of the fully assembled complex. The CW EPR spectrum of as-isolated MnxEF protein was reported previously⁸ and is reproduced in Figure 1 (orange trace, e). The spectrum contains signals from one class of T2Cu site with $g_{\parallel} = 2.210$, $^{63}\text{Cu } A_{\parallel} = 615$ MHz. The EPR spectrum of MnxEF also shows seven ^{14}N ($I = 1$) superhyperfine lines centered at $g = 2.046$, with an intensity ratio of $\approx 1:3:6:7:6:3:1$ and split by ≈ 1.5 mT (see simulation in Figure S8). The number and intensity pattern of these superhyperfine lines suggest that there are three ^{14}N -containing ligands to T2Cu sites in MnxEF protein.

Now by comparing the spectrum of the MnX protein complex without exogenous Cu(II) species (Figure 1, red trace) with the MnxEF spectrum, the signals of T2Cu sites in the isolated MnxEF protein (Figure 1, orange trace) are seen to match well with those of the T2Cu-B species (vide supra). Thus, we tentatively assign the T2Cu-B signals shown in the spectrum of the MnX protein complex to T2Cu sites in the MnxEF subunit. Spin quantification reveals that there are $\approx 3\text{Cu(II)}$ per MnxEF protein.

Some of the remaining copper centers in the isolated MnX protein complex can be selectively removed by a harsher,

Table 1. EPR Parameters of Type 2 Cu Sites in MCOs, Adapted from Ref 11

enzyme	subunits	MW (kDa)	g_{\parallel}	g_{\perp}	$^{63}\text{Cu } A_{\parallel}$ (MHz)	ref
plant laccase <i>Rhus succedanea</i>	1	130	2.241	2.054, 2.041	579	47
fungal laccase <i>Pleurotus ostreatus</i>	1	59–64	2.263	–	528	48
fungal laccase <i>Phlebia radiata</i>	1	64	2.25	–	510	49
ascorbate oxidase <i>Cucurbita pepo medullosa</i>	2	140	2.242	2.053	597	55
ascorbate oxidase <i>Acremonium</i> sp. HI-25	1	80	2.235	2.071	603	50
human ceruloplasmin	1	132	2.247	2.06	567	51
bilirubin oxidases	1	64	2.257	2.051	497	52
CueO	1	53	2.24	2.04	558	53
Fet3p	1	73	2.26	2.05	570	54
phenoxazinone synthase	6	540	2.34	2.07	480	40
Mnx complex	≈7	211	2.320	2.055	510	this work
MnxG	1	138	2.230	2.060	570	this work

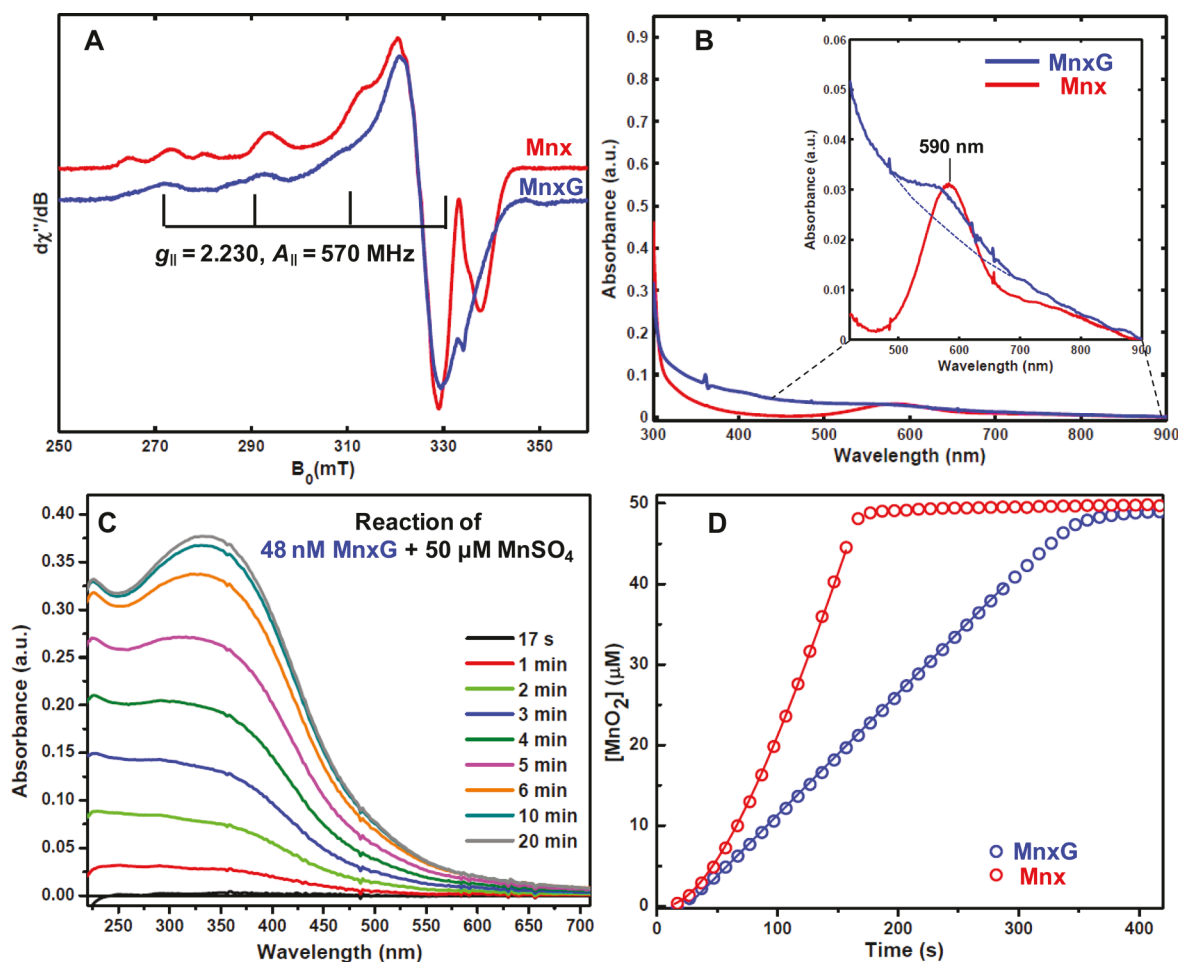


Figure 3. (A) X-band CW EPR spectra of the as-isolated Mnx complex (red trace) and the isolated MnxG protein (blue trace). Experimental parameters: temperature = 15 K; microwave frequency = 9.38 GHz; microwave power = 0.02 mW (no saturation); conversion time = 40 ms; modulation amplitude = 0.8 mT; and modulation frequency = 100 kHz. (B) UV-vis absorption spectra of 6 μM MnxG protein (blue trace) and 6 μM Mnx complex (red trace) at room temperature. The buffer is 20 mM HEPES, 20 mM NaCl, pH = 7.8, 20% ethylene glycol. Inset shows an expanded view of the absorption spectra in the 400–900 nm region. For MnxG protein, a baseline rising to shorter wavelengths (dashed blue line) likely results from protein aggregation. (C) UV-vis spectra taken at the indicated times during the MnxG-catalyzed oxidation of 50 μM MnSO_4 in 10 mM HEPES buffer (pH = 7.8) under UV-vis light at room temperature. (D) Time profile for the early product manganese oxide during 50 μM MnSO_4 oxidation by 48 nM MnxG (blue \circ) in 10 mM HEPES, pH = 7.8, which is monitored by the absorbance at 240 nm in (C) in order to minimize the effect of MnO_2 nanoparticle growth (resulting in a broad band ~ 350 nm, see [Experimental Procedures](#) for details). The red \circ show the time profile for early product manganese oxide during 50 μM MnSO_4 oxidation by 50 nM Mnx complex in 10 mM HEPES, pH = 7.8, with the corresponding UV-vis spectra shown in [Figure S12](#).

6 h long dialysis with a more concentrated (50 mM) Tris-HCl buffer solution [Cu(II) binding affinity to Tris is $4 \times 10^4 \approx 2 \times 10^6 \text{ M}^{-1}$ at pH 7.4].³⁹ After this so-called “harsh”

treatment, the protein shows no $\text{Mn}^{2+}(\text{aq})$ oxidation activity, and only one class of EPR signal remains with magnetic parameters $g_{\parallel} = 2.210$, $^{63}\text{Cu } A_{\parallel} = 615 \text{ MHz}$ ([Figure 1](#) magenta trace),

which match those of the T2Cu-B signal assigned above to T2Cu sites in the MnxEF subunit. Spin quantification reveals that there are ≈ 3 Cu(II) per Mnx complex after the harsh Tris-treatment; thus, the T2Cu sites in MnxEF protein remain intact in the Mnx complex after the harsh treatment dialysis. The harsh Tris treatment also bleaches the UV-vis feature (electronic absorption at 590 nm) corresponding to the oxidized T1Cu center in the MnxG unit.²⁷ These results suggest that both the T1Cu and T2Cu-A sites in the Mnx complex which are removed via dialysis are coordinated within the MnxG unit. Simulation of the total spectrum of Mnx (Figures 1 and 2) requires two equivalents of the T2Cu-A signal. One of these is, of course, the T2 site that is part of the trinuclear copper active site for O₂ reduction, although we note that the experimentally determined g_{\parallel} value (2.320) for the T2Cu-A sites is higher than the range of g_{\parallel} values (2.217–2.263) measured for T2Cu in other MCOs, like laccase, ascorbate oxidase, human ceruloplasmin, bilirubin oxidase, and Fet3p enzyme (Table 1). However, the g_{\parallel} value (2.320) for the T2Cu-A sites is comparable to the reported g_{\parallel} value (2.34) for both T2Cu sites in the MCO phenoxazinone synthase.^{11,40} Note that the authors⁴⁰ claimed that this T2Cu site in phenoxazinone synthase was not catalytically relevant, as its EPR signal was still observable after anaerobic incubation with substrates. There was, however, a 50% diminution of the T2Cu EPR signal intensity so perhaps its reduction to Cu(I) was merely incomplete. This high g_{\parallel} could be more consistent with the “alternative resting” form of the trinuclear copper active site ($g_{\parallel} = 2.34\text{--}2.39$, $^{63}\text{Cu } A_{\parallel} = 240\text{--}300$ MHz);^{41,42} however, we rule this out as there are no differences in Cu(II) EPR signals between the as-isolated Mnx and fully reduced Mnx that has been reoxidized by oxygen (Figure S9). The other T2Cu-A center must be located within MnxG or at the interface between MnxG and the MnxEF unit. The T2Cu site in the trinuclear site of other MCOs is coordinated by two histidine imidazole groups and a hydroxide-(water) molecule. That the two T2Cu-A signals are so similar may imply that the corresponding metal centers have similar coordination environments, although there is yet no X-ray structure of Mnx.

When six equivalents of Cu(II) are added to the colorless harshly Tris-treated Mnx protein complex, the blue color from T1Cu sites (electronic absorption at 590 nm) as well as T2Cu-A signals in EPR spectrum returns, giving the same spectra as for the as-isolated Mnx protein complex (Figure S10, red trace). Additionally, when ethylenediaminetetraacetic acid (EDTA), which has higher binding affinity for Cu(II) ($\approx 5 \times 10^{18} \text{ M}^{-1}$ at 25 °C), was included in the dialysis buffer, all three classes of EPR signals were seen to diminish in intensity, but they did not disappear entirely ($\approx 0.3\text{Cu(II)}/\text{Mnx}$ remains after 3 h dialysis, data not shown).

The EPR spectrum of the isolated MnxG protein is shown in Figure 3A (blue trace). T2Cu signals are observable with $g_{\parallel} = 2.230$, $A_{\parallel} = 570$ MHz, values that falls in the range for the T2Cu in other MCOs. However, the T2Cu signals in the isolated MnxG are different from the T2Cu-A signals identified in the full Mnx complex (Table 1). This perhaps suggests that in the absence of the MnxEF subunit, the structure of MnxG is distorted to such an extent that the T2Cu-A sites associated with MnxG are perturbed. Spin quantification reveals that there are ≈ 2 EPR-detectable Cu(II) ions per MnxG unit (not including the EPR-silent T3Cu sites). However, there is no apparent T1Cu signal in the corresponding EPR spectrum. This lack of signal could result from the T1Cu site being

incompletely loaded in the isolated MnxG protein. The electronic absorption spectrum of MnxG shows a small peak at λ_{590} that sits upon a baseline rising toward shorter wavelengths that likely results from aggregated MnxG forming particulates and leading to light scattering. Subtracting off this baseline leads to a peak with intensity of 0.013 a.u. Using the extinction coefficient for the full Mnx complex ($\epsilon_{590} = 5600 \text{ M}^{-1} \text{ cm}^{-1}$) determined in this study (Figure 3B), the occupancy of the T1Cu site of isolated MnxG protein is estimated to be $\sim 40\%$. The expected corresponding EPR signal of these T1Cu sites are obscured by the strong signals from T2Cu centers bound to MnxG (Figure 3A).

Importantly, the isolated MnxG protein shows Mn²⁺(aq) oxidation activity (Figure 3C,D) and Figure S11), with the apparent steady-state rate V_{s-s} ca. $0.150 \mu\text{M s}^{-1}$ (see Experimental Procedure for details of the fitting). The rate of MnxG-catalyzed MnO_x formation is slower than the rate of MnO_x formation catalyzed by Mnx complex with V_{s-s} ca. $0.513 \mu\text{M s}^{-1}$ (see Figure 3D and ref 30) but much faster than abiotic MnO_x formation. The slower rate MnxG-catalyzed MnO_x formation could be due to the partial occupancy of T1Cu site in MnxG. We note that the initial lag time of the reaction appear to be very similar to one another. However, after approximately 30 s, the rate of Mn-oxidation by the full Mnx complex accelerates by a factor of 3, indicating some type of activation has occurred. Note that these kinetic traces are the sum of two processes: enzymatic MnO₂ formation and subsequent MnO₂ nanoparticle growth, and a more detailed investigation is underway to deconvolute these two processes for direct comparison with the Mnx complex.

To simulate the total EPR spectrum of as-isolated Mnx, we consider the following observations. Spin quantification of the EPR signal for the Mnx complex indicates that six mononuclear Cu(II) sites contribute. Three of these copper sites (T2Cu-B species) are found in the MnxEF subunit, as illustrated in Figure 4 and Table 2. Thus, there should be three mononuclear Cu(II) sites associated with MnxG subunit. The gene sequence indicates that there is only one T1Cu site (with the predicted ligands as His340, His281, Cys335, and Met345),⁹ leaving two T2Cu sites (T2Cu-A species) in the MnxG unit. One putative T2Cu site (with His284, His529, and aquo-derived hydroxo as ligands)⁹ is adjacent to the putative T3Cu site and is part of the trinuclear cluster that reduces O₂ to water (vide supra). The extra T2Cu site in the MnxG unit could have His1134 as one ligand, according to a previous gene alignment.⁹ Although the function of this putative extra T2Cu site is unknown, it could be structurally relevant as an extra T2Cu site is also found in the MCO enzyme phenoxazinone synthase, where it helps to stabilize the quaternary structure of the homohexamer.²³ Given these results, we simulate the spectrum of the Mnx protein complex as a sum of three distinct Cu(II) species, employing a ratio of T2Cu-A:T2Cu-B:T1Cu 2:3:1, as shown in Figures 1 and 2.

As described above, the addition of Tris or EDTA was shown to chelate out certain copper centers in the Mnx complex leading to a diminution of the corresponding EPR signals. In what follows, we use Fe(II) [in the form of (NH₄)₂Fe(SO₄)₂] to chemically reduce certain Cu(II) sites to Cu(I), thus turning off their contribution to the EPR spectrum (Figure S13). Treating as-isolated Mnx protein anaerobically with 6 equiv of (NH₄)₂Fe(SO₄)₂ leads to a reduction of some T2Cu-A centers. Indeed, the “WT Mnx”-minus-“6Fe(II) + Mnx” difference spectrum is well-simulated using the T2Cu-A magnetic

Importantly, isolated MnxG and the full Mnx complex exhibit nearly identical lag phase during the manganese-oxidation reaction (Figure 3D), but after several seconds, the rate increases 3-fold in the Mnx-catalyzed reaction. These results could suggest that the MnxEF complex is participating in an activation mechanism to enhance enzymatic activity or MnO₂ formation. One possibility is that the T2Cu-B sites are involved in the conduction of oxidizing equivalents to the protein exterior for formation of bulk MnO_x. Such a mechanism is consistent with our previous hypothesis that the multiple manganese and copper centers in Mnx (and perhaps redox-active amino acids such as tyrosine) could form a wire to the protein surface in order to prevent solid MnO_x from occluding the active site.^{7,8,27}

From our earlier freeze-quench EPR study of the Mnx-catalyzed Mn-oxidizing activity (Figure 5),²⁷ we observed changes in the various Cu(II) EPR signals as a function of reaction time after mixing O₂-containing buffer with a

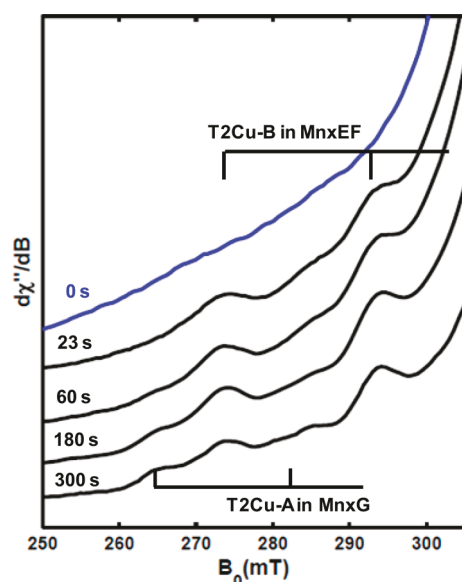


Figure 5. Expanded view of $g_{||}$ -region of X-band CW EPR spectra of freeze-quenched mixtures (aging time given in figure) of dithionite-reduced Mnx complex [preincubated with 4 equiv of Mn²⁺(aq)] reacted with O₂-saturated buffer. Spectra are the same as those published in Figure 3 of ref 27.

Mn(II)-containing solution of dithionite-reduced Mnx complex. With assignments for these signals now in hand, we can make the following observations: the T2Cu-B sites in the MnxEF subunit are oxidized shortly after mixing (earliest time point in that study was 23 s). These copper sites remain oxidized throughout the reaction (monitored up to 300 s). Meanwhile, the T2Cu-A signal ascribed to MnxG only appears after the reaction with O₂ has proceeded for approximately 60 s, coinciding with the loss of the sharp sextet corresponding to aqueous Mn(II).²⁷ These results seem to suggest that the T2Cu-B sites in the MnxEF subunit can be oxidized by O₂ but not reduced by the Mn(II) substrate and, once oxidized, remain so at steady-state. By contrast, the T2Cu-A site in MnxG only gets oxidized once substrate Mn(II) is exhausted. The residual Mn(II) signals that we observe after long reaction times, may correspond to Mn(II) bound somewhere to the MnxEFG complex but are unreactive.

Now that MnxG and the MnxEF hexamer can be expressed and studied independently, progress toward determining the

precise roles of the protein subunits and their metal cofactors should be forthcoming.

■ ASSOCIATED CONTENT

Supporting Information

The Supporting Information is available free of charge on the ACS Publications website at DOI: 10.1021/jacs.7b02277.

Procedures of spin quantification, SDS-PAGE gels following protein expression via various *mnx* gene constructs; Q-band CW EPR spectrum of the as-isolated Mnx protein complex; X-band CW EPR spectra of Mnx protein complex treated with Fe(II); X-band CW EPR spectra of the Mnx protein complex treated with H₂O₂; and X-band CW EPR spectra of Mnx protein complex showing various copper complementation; photographs showing manganese oxides; and UV-vis (PDF)

■ AUTHOR INFORMATION

Corresponding Author

*rdbritt@ucdavis.edu.

ORCID

Shu-Hao Liou: 0000-0002-9716-6108

Alexandra V. Soldatova: 0000-0003-2876-6262

William H. Casey: 0000-0002-3275-6465

R. David Britt: 0000-0003-0889-8436

Notes

The authors declare no competing financial interest.

■ ACKNOWLEDGMENTS

The work was supported by the National Science Foundation award numbers CHE-1213699 and CHE-1665455 to R.D.B., EAR-1231322 to W.H.C., CHE-1410688 to B.M.T., CHE-1410353 to T.G.S. and an NSF Postdoctoral Research Fellowship in Biology Award ID: DBI-1202859 to C.A.R. The EPR spectrometers at the CalEPR facility used in this study were funded by the National Institutes of Health (S10-RR021075) and the NSF (CHE-1048671).

■ REFERENCES

- (1) Post, J. E. *Proc. Natl. Acad. Sci. U. S. A.* **1999**, *96*, 3447.
- (2) *Photoredox Transformation of Iron and Manganese in Marine Systems: Review of Recent Field Investigations*; Waite, T. D., Szymczak, R., Eds.; Lewis Publishers: London, 1994.
- (3) Sunda, W. G.; Huntsman, S. A. *Deep-Sea Res., Part A* **1988**, *35*, 1297.
- (4) Spiro, T. G.; Bargar, J. R.; Sposito, G.; Tebo, B. M. *Acc. Chem. Res.* **2010**, *43*, 2.
- (5) Tebo, B. M.; Bargar, J. R.; Clement, B. G.; Dick, G. J.; Murray, K. J.; Parker, D.; Verity, R.; Webb, S. M. *Annu. Rev. Earth Planet. Sci.* **2004**, *32*, 287.
- (6) Morgan, J. J. *Geochim. Cosmochim. Acta* **2005**, *69*, 35.
- (7) Butterfield, C. N.; Soldatova, A. V.; Lee, S. W.; Spiro, T. G.; Tebo, B. M. *Proc. Natl. Acad. Sci. U. S. A.* **2013**, *110*, 11731.
- (8) Butterfield, C. N.; Tao, L.; Chacon, K. N.; Spiro, T. G.; Blackburn, N. J.; Casey, W. H.; Britt, R. D.; Tebo, B. M. *Biochim. Biophys. Acta, Proteins Proteomics* **2015**, *1854*, 1853.
- (9) Dick, G. J.; Torpey, J. W.; Beveridge, T. J.; Tebo, B. M. *Appl. Environ. Microbiol.* **2008**, *74*, 1527.
- (10) van Waasbergen, L. G.; Hildebrand, M.; Tebo, B. M. *J. Bacteriol.* **1996**, *178*, 3517.
- (11) Solomon, E. I.; Sundaram, U. M.; Machonkin, T. *Chem. Rev.* **1996**, *96*, 2563.

- (12) Solomon, E. I.; Szilagy, R. K.; DeBeer George, S.; Basumallick, L. *Chem. Rev.* **2004**, *104*, 419.
- (13) Heppner, D. E.; Kjaergaard, C. H.; Solomon, E. I. *J. Am. Chem. Soc.* **2013**, *135*, 12212.
- (14) Machonkin, T. E.; Solomon, E. I. *J. Am. Chem. Soc.* **2000**, *122*, 12547.
- (15) Quintanar, L.; Gebhard, M.; Wang, T. P.; Kosman, D. J.; Solomon, E. I. *J. Am. Chem. Soc.* **2004**, *126*, 6579.
- (16) Heppner, D. E.; Kjaergaard, C. H.; Solomon, E. I. *J. Am. Chem. Soc.* **2014**, *136*, 17788.
- (17) Li, J.; Farrokhnia, M.; Rulíšek, L.; Ryde, U. *J. Phys. Chem. B* **2015**, *119*, 8268.
- (18) Lindley, P. F.; Zaitseva, I.; Zaitsev, V.; Reinhammar, B.; Selin-Lindgren, E.; Yoshida, K.; Card, G. *J. Biol. Inorg. Chem.* **1997**, *2*, 454.
- (19) Djoko, K. Y.; Chong, L. X.; Wedd, A. G.; Xiao, Z. *J. Am. Chem. Soc.* **2010**, *132*, 2005.
- (20) Singh, S. K.; Roberts, S. A.; McDevitt, S. F.; Weichsel, A.; Wildner, G. F.; Grass, G. B.; Rensing, C.; Montfort, W. R. *J. Biol. Chem.* **2011**, *286*, 37849.
- (21) Roberts, S. A.; Wildner, G. F.; Grass, G.; Weichsel, A.; Ambrus, A.; Rensing, C.; Montfort, W. R. *J. Biol. Chem.* **2003**, *278*, 31958.
- (22) Roberts, S. A.; Weichsel, A.; Grass, G.; Thakali, K.; Hazzard, J. T.; Tollin, G.; Rensing, C.; Montfort, W. R. *Proc. Natl. Acad. Sci. U. S. A.* **2002**, *99*, 2766.
- (23) Smith, A. W.; Camara-Artigas, A.; Wang, M.; Allen, J. P.; Francisco, W. A. *Biochemistry* **2006**, *45*, 4378.
- (24) Romano, C. A.; Zhou, M.; Song, Y.; Wysocki, V.; Dohnalkova, A.; Kovarik, L.; Paša-Tolić, L.; Tebo, B. M. *Nat. Commun.*, submitted for publication, **2017**.
- (25) Butterfield, C. N. Characterizing the Mn (II) Oxidizing Enzyme from the Marine Bacillus Sp. PL-12 Spore. Ph.D Thesis, Oregon Health & Science University, 2014.
- (26) Tao, L.; Simonov, A. N.; Romano, C. A.; Butterfield, C. N.; Fekete, M.; Tebo, B. M.; Bond, A. M.; Spiccia, L.; Martin, L. L.; Casey, W. H. *Chem. - Eur. J.* **2017**, *23*, 1346.
- (27) Tao, L.; Stich, T. A.; Butterfield, C. N.; Romano, C. A.; Tebo, B. M.; Casey, W. H.; Britt, R. D.; Spiro, T. G. *J. Am. Chem. Soc.* **2015**, *137*, 10563.
- (28) Durão, P.; Chen, Z.; Fernandes, A. T.; Hildebrandt, P.; Murgida, D. H.; Todorovic, S.; Pereira, M. M.; Melo, E. P.; Martins, L. O. *J. Biol. Inorg. Chem.* **2008**, *13*, 183.
- (29) Webb, S. M.; Dick, G. J.; Bargar, J. R.; Tebo, B. M. *Proc. Natl. Acad. Sci. U. S. A.* **2005**, *102*, 5558.
- (30) Soldatova, A. V.; Tao, L.; Romano, C. A.; Stich, T. A.; Casey, W. H.; Britt, R. D.; Tebo, B. M.; Spiro, T. G. *J. Am. Chem. Soc.*, submitted for publication, **2017**.
- (31) Grady, J. K.; Chasteen, N. D.; Harris, D. C. *Anal. Biochem.* **1988**, *173*, 111.
- (32) Zhao, G.; Chasteen, N. D. *Anal. Biochem.* **2006**, *349*, 262.
- (33) Good, N. E.; Winget, G. D.; Winter, W.; Connolly, T. N.; Izawa, S.; Singh, R. M. M. *Biochemistry* **1966**, *5*, 467.
- (34) Soldatova, A. V.; Oyerinde, O. F.; Balakrishnan, G.; Romano, C. A.; Tebo, B. M.; Spiro, T. G. *manuscript in preparation*.
- (35) Carithers, R. P.; Palmer, G. *J. Biol. Chem.* **1981**, *256*, 7967.
- (36) Stoll, S.; Britt, R. D. *Phys. Chem. Chem. Phys.* **2009**, *11*, 6614.
- (37) Stoll, S.; Schweiger, A. *J. Magn. Reson.* **2006**, *178*, 42.
- (38) Solomon, E. I.; Heppner, D. E.; Johnston, E. M.; Ginsbach, J. W.; Cirera, J.; Qayyum, M.; Kieber-Emmons, M. T.; Kjaergaard, C. H.; Hadt, R. G.; Tian, L. *Chem. Rev.* **2014**, *114*, 3659.
- (39) Nagaj, J.; Stokowa-Sołtys, K.; Kurowska, E.; Frączyk, T.; Jeżowska-Bojczuk, M.; Bal, W. *Inorg. Chem.* **2013**, *52*, 13927.
- (40) Freeman, J. C.; Nayar, P. G.; Begley, T. P.; Villafranca, J. J. *Biochemistry* **1993**, *32*, 4826.
- (41) Kjaergaard, C. H.; Jones, S. M.; Gounel, S.; Mano, N.; Solomon, E. I. *J. Am. Chem. Soc.* **2015**, *137*, 8783.
- (42) Kjaergaard, C. H.; Durand, F.; Tasca, F.; Qayyum, M. F.; Kauffmann, B.; Gounel, S. b.; Suraniti, E.; Hodgson, K. O.; Hedman, B.; Mano, N.; Solomon, E. I. *J. Am. Chem. Soc.* **2012**, *134*, 5548.
- (43) Ballhausen, C. J. *Introduction to Ligand Field Theory*; McGraw-Hill: New York, 1962.
- (44) Mabbs, F. E.; Collison, D. *Electron Paramagnetic Resonance of d Transition Metal Compounds*; Elsevier Science: Amsterdam, 1992.
- (45) Gerloch, M.; Miller, J. R. *In Progress in Inorganic Chemistry*; John Wiley & Sons, Inc.: New York, 1968; Vol. 10.
- (46) Branden, R.; Deinum, J. *Biochim. Biophys. Acta* **1978**, *524*, 297.
- (47) Quintanar, L.; Yoon, J.; Aznar, C. P.; Palmer, A. E.; Andersson, K. K.; Britt, R. D.; Solomon, E. I. *J. Am. Chem. Soc.* **2005**, *127*, 13832.
- (48) Youn, H.-D.; Kim, K.-J.; Maeng, J.-S.; Han, Y.-H.; Jeong, I.-B.; Jeong, G.; Kang, S.-O.; Hah, Y. C. *Microbiology* **1995**, *141*, 393.
- (49) Karhunen, E.; Niku-Paavola, M.-L.; Viikari, L.; Haltia, T.; van der Meer, R. A.; Duine, J. A. *FEBS Lett.* **1990**, *267*, 6.
- (50) Hirose, J.; Sakurai, T.; Imamura, K.; Watanabe, H.; Iwamoto, H.; Hiromi, K.; Itoh, H.; Shin, T.; Muraio, S. *J. Biochem.* **1994**, *115*, 811.
- (51) Gunnarsson, P.-O.; Nylén, U.; Pettersson, G. *Eur. J. Biochem.* **1973**, *37*, 47.
- (52) Hiromi, K.; Yamaguchi, Y.; Sugiura, Y.; Iwamoto, H.; Hirose, J. *Biosci., Biotechnol., Biochem.* **1992**, *56*, 1349.
- (53) Kataoka, K.; Sugiyama, R.; Hirota, S.; Inoue, M.; Urata, K.; Minagawa, Y.; Seo, D.; Sakurai, T. *J. Biol. Chem.* **2009**, *284*, 14405.
- (54) Hassett, R. F.; Yuan, D. S.; Kosman, D. J. *J. Biol. Chem.* **1998**, *273*, 23274.
- (55) Marchesini, A.; Kroneck, P. M. N. *Eur. J. Biochem.* **1979**, *101*, 65.
- (56) Majumdar, S.; Lukk, T.; Solbiati, J. O.; Bauer, S.; Nair, S. K.; Cronan, J. E.; Gerlt, J. A. *Biochemistry* **2014**, *53*, 4047.